RESEARCH ARTICLE | FEBRUARY 05 2024

Flow induced rigidity percolation in shear thickening suspensions

Abhay Goyal ; Nicos S. Martys; Emanuela Del Gado

J. Rheol. 68, 219–228 (2024)
https://doi.org/10.1122/8.0000786
CHORUS

Flow induced rigidity percolation in shear thickening suspensions

Abhay Goyal,[1,2] Nicos S. Martys,[1] and Emanuela Del Gado[2,a)]

[1]*Infrastructure Materials Group, Engineering Laboratory, National Institute of Standards and Technology, Gaithersburg, MD, 20899*
[2]*Dept of Physics, Institute of Soft Matter Synthesis and Metrology, Georgetown University, Washington DC 20057*

(Received 3 November 2023; final revision received 10 January 2024; published 5 February 2024)

Abstract

Discontinuous shear thickening (DST) is associated with a sharp rise in a suspension's viscosity with increasing applied shear rate or stress. Key signatures of DST, highlighted in recent studies, are the very large fluctuations of the measured stress as the suspension thickens with increasing rate. A clear link between microstructural development and the dramatic increase in stress fluctuations has not been established yet. To identify the microstructural underpinnings of this behavior, we perform simulations of sheared dense suspensions. Through an analysis of the particle contact network, we identify a subset of constrained particles that contributes directly to the rapid rise in viscosity and large stress fluctuations. Indeed, both phenomena can be explained by the growth and percolation of constrained particle networks—in direct analogy to rigidity percolation. A finite size scaling analysis confirms this to be a percolation phenomenon and allows us to estimate the critical exponents. Our findings reveal the specific microstructural self-organization transition that underlies DST. https://doi.org/10.1122/8.0000786

I. INTRODUCTION

Suspensions, such as colloids, pharmaceuticals, slurries, and concrete, are central to several environmental and technological processes. Their flows exhibit phenomena ranging from shear thinning and thickening to thixotropy, giant stress fluctuations, and jamming [1,2]. In particular, discontinuous shear thickening (DST) is ubiquitous and dramatic, with a rapid rise in stress or viscosity as the applied shear rate increases (or a sudden shear rate decrease for stress driven shear). During DST, the flow becomes dilatant [3–5] and erratic, with giant stress fluctuations in response to the increasing shear rate [6–10]. The bulk rheology becomes sensitive to surface interactions, roughness, and hence frictional contacts between particles [11–14], in spite of the presence of solvent lubrication forces [5,15–21]. However, while particle surface contacts are strongly material and chemistry dependent, the overall DST phenomenology is consistent across all suspensions. The theoretical mean-field approach of Wyart and Cates [13], in which the microstructure is characterized by the suspension volume fraction and the overall fraction of frictional contacts produced under shear, demonstrated that the origin of DST rheology does not depend on the specifics of the material and surface chemistry. The large fluctuations of the shear stresses and the scaling properties of the shear response, observed over a wide range of suspensions [7–10,22,23], are reminiscent of collective processes in critical phenomena. Together these findings suggest that larger microstructures, made of many particles and built under shear, underpin DST [24–26].

More specifically, there is evidence, from both experiments and simulations, that spanning clusters or chains of particles carry large stresses during thickening [11,13,27–30]. We hypothesize that these or related structures may intermittently jam under flow, causing the abrupt stress fluctuations and raising the prospect of an underlying percolation transition. The sharp increase of the viscosity could signal the growth of a percolating, load-bearing microstructure, whose dynamics under shear would be at the origin of the giant stress fluctuations. With respect to order-disorder transitions highlighted in studies of flowing suspensions [31–34], the build-up of a percolating structure responsible for stress transmission, akin to a rigidity percolation [35–37], requires a more complex self-organization process, which is nearly undetectable in experiments but possibly recognizable in particle based simulations.

Computational studies that identify and characterize percolation transitions strongly depend on the capability to perform large scale simulations because a limited system size can make it impossible to follow the growth of the percolating structure [38]. Moreover, recognizing a disordered rigid structure embedded in a 3*d* disordered environment that may or may not contribute to its rigidity is a formidable challenge, even when considering a system at rest. For a shear thickening suspension, which is typically subjected to high shear rates or stresses, the conditions to directly test for mechanical rigidity are highly non trivial even for simulation studies. Hence, addressing such questions requires dedicated and extensive numerical resources. Recent simulation studies have analyzed a variety of geometrical motifs in the particle force contact networks that emerge during DST [25], including structures that would be rigid at rest [26], but did not find evidence of a percolation transition. A significant knowledge gap, therefore, still remains, as to whether a percolation growth underpins DST and its rheological signatures.

a)Author to whom correspondence should be addressed; electronic mail: emanuela.del.gado@georgetown.edu

Here, we use large scale 3D simulations of model suspensions to provide evidence that a percolation transition is indeed at the origin of the stress fluctuations characteristic of DST. The evidence is obtained once the basic unit of the microstructure that forms the percolating, stress bearing, network is identified in terms of locally overconstrained particles that share frictional contacts. The percolation of this microstructure can be directly linked to DST, and to the accompanying large stress fluctuations, and points to the role of rigidity percolation in this phenomenon. The growth and percolation of locally overconstrained particle clusters follow a critical behavior akin to the one of equilibrium systems close to a critical point, and can be studied via a finite size scaling analysis, which allows us to estimate the related critical exponents.

II. METHODS

We have utilized a model suspension of spheres that interact via hydrodynamic lubrication, contact repulsion, and frictional forces, following recent work on simulations of shear thickening [34,39,40]. The steric repulsion between particles is modeled as a Hookean force, depending on the surface separation h and a spring constant k, lubrication forces are regularized at short distances between the particle surfaces, and Coulomb friction acts tangentially on surface contacts (see details in Sec. II A). All spheres have the same size, while all interaction parameters have been adjusted to match the model in [40]. We integrate the equations of motion for all particles as in [34], performing simulations of large systems with LAMMPS (Large-scale Atomic/Molecular Massively Parallel Simulator) [41] with overdamped particle motions. The suspension is subject to thermal fluctuations and sheared using Lees–Edwards boundary conditions and imposing a constant shear rate with a background velocity field that particle motion can relax to.

All quantities are reported in reduced units as a combination of basic units: energy scale $\varepsilon = k_B T$, particle mass m whose effect is damped by the solvent viscosity η_0, and particle diameter d. While the natural time unit used in the simulations is the inertial time $\tau_0 = \sqrt{md^2/\epsilon}$, we are solving the equations of motions in the overdamped limit and in the following the shear rate $\dot{\gamma}$ is, therefore, scaled by a characteristic rate $\dot{\gamma}_0$ at which the drag force due to the solvent becomes on the order of a characteristic force at contact [42]. Here, we use $\dot{\gamma}_0 = k_0\delta/6\pi\eta_0 d^2$, where $6\pi\eta_0 d^2$ is the drag force due to the solvent of viscosity η_0, k_0 is the characteristic spring constant describing the contact mechanics, and we estimate the characteristic force at contact $k_0\delta$ when two particles numerically have an overlap $\delta \approx 10^{-6}$ of their diameter d.

In this work, we present data on particle volume fraction $\phi = 56\%$, reproducing the same DST features as in [40], but with the number of particles N ranging between 1687 and 45 528 and the simulation box size between $11.64d$ and $34.92d$. When not explicitly indicated, the data always refer to the largest system size.

A. Simulation details

All simulations were performed with LAMMPS [41]. While generally known for molecular dynamics simulations, the LAMMPS code has specialized modules that allow for the modeling of soft sphere suspensions of Brownian particles. For this application, LAMMPS utilizes a physics-based discrete element method (DEM) model that simplifies the detailed flow behavior of the suspension solvent in exchange for computational efficiency. Hydrodynamic interactions between spheres are largely controlled by lubrication forces. Shear flow was imposed along the x direction (with gradient along z) based on the Lees–Edwards boundary condition, with an additional Stokesian drag force which causes particles to follow the imposed shear profile over time. The robustness of this approach improves with increasing volume fraction of spheres as a less detailed knowledge of flow of the background fluid is needed. Indeed, it has been found that at volume fractions of approximately 40 % and higher, the flows produced are reasonably consistent with fully detailed simulations [43]. This is due to the fact that, at higher volume fractions, the surfaces of the solid inclusions are close enough such that the lubrication forces dominate over the long-range hydrodynamics of the background fluid [44]. A detailed description of this approach can be found in our previous paper [34].

In addition to the hydrodynamic forces, frictional forces are included following the contact model of Mari *et al.* [11,12] The steric repulsion between particles is modeled as a Hookean force, with a normal force of $F_N = kh$ that depends only on particle surface separation h and spring constant k. This allows for particle contact, which is the criterion for activating frictional forces. As in [11,12], to mimic a hard contact, we use a high spring constant of $k = k_0\dot{\gamma}$, with k_0 values between 10^7 and 10^8 in our reduced units. With these parameters, we observe particle overlap always $<3\%$, comparable to the criteria used in other recent simulations [45]. The dependence on the shear rate arises from the fact that a higher spring constant is needed to limit overlap at higher shear rates due to collisions happening more frequently and at greater velocities. Alternatively, one could use a fixed, high value of k, corresponding to what is required for the highest shear rate, at all rates. However, this requires a smaller timestep to adequately resolve collisions, and the variable spring constant approach was found to reduce computational cost while producing results that matched the results from the constant k approach [45].

The frictional forces act tangentially to the particle contact and also follow a simple Hookean model. Any tangential displacement of particles after making contact, Δr_t, is acted upon by a restoring frictional force $F_t = k\Delta r_t$, with the constraint that $F_t \leq F_N$ (Coulomb's friction law with a friction coefficient of 1). The contact/friction model we use is relatively simple compared to some recent studies that have explicitly included a more detailed description of the particle surface roughness [17,20], which produces the frictional contacts. However, for all these models the DST exhibits similar behavior, and the simpler model also compares favorably with experiments [46]. While a more detailed study of the different contact models is beyond the scope of this work, we note that the recent studies that use rolling friction [47], or hydrodynamic interactions with surface roughness [17,20], as

the main microscopic mechanism for frictional contacts, find a shift in the DST onset but, overall, recover the same DST phenomenology obtained with sliding friction and simpler contact laws. On this basis, a more detailed and complex contact model is needed to quantitatively predict the value of the stress or shear rate corresponding to the DST onset, but it is not expected to significantly change the nature of the microstructural growth underpinning the rheology.

B. Data analysis

Simulations for all system sizes were run for at least 40 strain units to ensure sufficient sampling of the steady state flow. The data shown, except in cases where it is plotted as a function of γ, are averages over all sampled points with $\gamma > 10$. The error bars correspond to the standard deviation of the average and are smaller than the symbol size when not visible.

The stress is calculated from the particle contributions to the stress tensor, following [48], as

$$\sigma_{\alpha\beta} = -\frac{1}{V}\sum_i \left[\sum_{j\neq i}\left(\frac{1}{2}F^{ij}_{\alpha}r^{ij}_{\beta}\right) - mv^i_{\alpha}v^i_{\beta}\right], \tag{1}$$

where α and β can be x, y, or z to generate the components of the stress tensor, V is the system volume, $\vec{F}^{ij}$ and $\vec{r}^{ij}$ are the force and position vectors between particles i and j, and $\vec{v}^i = \vec{v}^i_{\text{total}} - \dot{\gamma}z\hat{x}$ is the deviation of the particle velocity from the flow profile set by the shear rate. The suspension viscosity is computed from the shear stress σ_{xz} and shear rate $\dot{\gamma}$ as $\eta = \sigma_{xz}/\dot{\gamma}$.

For the clustering analysis, particles are considered connected when they are in contact. In our simulation model, the contact can be exactly determined by a distance threshold between particle centers: $r_{ij} < d$ means particles overlap, experience steric repulsion, and are frictionally constrained. We have verified that particles experiencing *slipping contacts*, i.e., contacts precisely at the Coulomb threshold, are statistically negligible. We identify particles with at least k contacts (k-neighbor particles) and clusters of them. After sorting the particles, clusters of k-neighbor particles can be identified by searching for contacts between k-neighbor particles. k-neighbor particles and their clusters may seem quite similar to k-core clusters used in network theory to characterize connectivity patterns in random networks and recently employed in the forced contact network analysis close to DST [25]. However, k-core clusters are defined using subgraphs of the initial contact network in which all member particles have k or more frictional contacts with other members of the same subgraph. In k-neighbor clusters, instead, all member particles have k or more frictional contacts. That is, particles belonging to k-neighbor clusters have k or more frictional contacts but not necessarily with particles in the same clusters, i.e., the contact particles may have fewer than k contacts (see Fig. 1). The difference in the two definitions may appear subtle but is important, as it will appear in our analysis in Sec. III. In fact, k-core structures select particles on the basis of their degree of connectivity

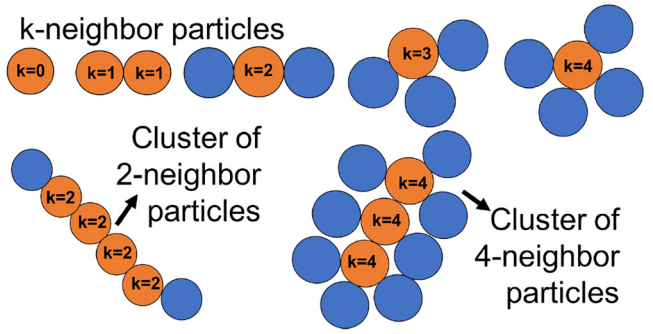

FIG. 1. A 2D schematic representation of what we refer to as k-neighbor particles and examples of clusters they may form. All the simulations reported here are in 3D.

(e.g., all particles in a cluster have the same connectivity), whereas k-neighbor structures end up selecting for local geometry of particles (independently from how low or high the connectivity of their neighbors is). With using k-neighbor particle clusters, our hypothesis is that the local geometric arrangement of the particles in a cluster, signaled by their number of neighbors, can be a proxy for local rigidity and mechanical stability. This hypothesis will be supported by the results obtained. We provide a simple 2D visualization of k-neighbor particles and the clusters they can form (Fig. 1).

For each k, the whole distribution of possible cluster sizes is obtained from each simulation snapshot, with the size being the "mass," i.e., the number s of particles which satisfy the criterion chosen and belong to the same cluster, as usually done in percolation problems [38]. The cluster size distribution indicates the number of clusters of a given size s per particle. To sort the clusters efficiently and obtain the complete cluster size distributions for each k and for all shear rates considered, we use the Hoschen–Kopelman algorithm [49]. Once the cluster analysis is completed, a cluster of k-neighbor particles is defined to be percolating in a direction if, when we split our system into thin ($< .45d$) slices along that axis, at least 1 particle from the cluster is in each slice. The percolation probability R at any given $\dot{\gamma}$ is computed as the fraction of sampled γ values at which a percolating cluster exists. The probability P of a particle being in the percolating cluster is determined from the number of particles in the percolating cluster compared to the total N.

From all non-percolating clusters and their size distributions computed at each shear rate $\dot{\gamma}$, k value, and at each strain γ, we compute the size of the largest clusters $S_{\max}$ and average it over the whole strain window available. The mean cluster size S is the second moment of the cluster size distribution, given as

$$S = \sum_s s^2 n_s, \tag{2}$$

where s is a cluster size and n_s is the cluster size distribution (i.e., number of clusters of size s normalized by N) obtained for a given k value, at each shear rate, and for each γ. Also here, we average S over the whole strain window.

Finally, to visualize local contributions to the overall stress, the virial formulation of the stress tensor is broken up into particle contributions as

$$\sigma^i_{\alpha\beta} = -\sum_{j\neq i}\left[\frac{1}{2}F^{ij}_{\alpha}r^{ij}_{\beta}\right] - mv^i_{\alpha}v^i_{\beta} \tag{3}$$

and the particle contribution to the total are colored according to their magnitude.

III. RESULTS

A. DST and stress fluctuations

As mentioned above, the data reported here refer to simulation boxes containing 1688, 13 500, and 45 563 spheres, with edge length, L= 11.64 d, 23.28 d, and 34.92 d, respectively. The medium and larger sizes are much larger than in the previous studies, which is essential to address the critical-like behavior of stress fluctuations and to deal with the finite-size effects typical of percolation transitions. We use the convention that x corresponds to the flow direction, y to the vorticity direction, and z to the shear gradient direction.

We use the shear component σ_{xz} of the stress tensor, obtained from interparticle forces, relative positions, and particle velocities [Eq. (3)] [50] to extract the relative viscosity η_r, plotted in Fig. 2(a) as a function of the shear rate $\dot{\gamma}$ for the three system sizes. The data show a steep increase in viscosity at a threshold shear rate $\dot{\gamma} \simeq 5$, and increasing the system size confirms the sharp viscosity increase, indicating that DST here is not an artifact of limited sample sizes used in simulations. The shear stress distributions, extracted from the time series, are Gaussian at low rates, but, as $\dot{\gamma}$ approaches DST, they develop exponential tails consistent with experiments [10]. The non-Gaussian tails are more pronounced for the larger system sizes, indicating that the large stress fluctuations and their non-Gaussian nature are not merely the result of limited statistics. The time series from which the viscosity is extracted in the steady state are plotted in Fig. 2(b), showing (for the intermediate system size of 13 500 particles) $\sigma_{xz}/\dot{\gamma}$ as a function of the strain γ for several shear rates. The data clearly feature large fluctuations of shear stress at DST.

Previous work [25] has shown that, close to shear thickening, the shear stress increases with the mean number of frictional contacts per particle, which peaks at 3 and 4 for large shear rates. However, in terms of the mean frictional contact number, a distinction could not be made between continuous shear thickening (CST) and DST, whereas they clearly have different rheological signatures. These findings support the idea that not just the mean frictional contact number but rather the local microstructural environment and its larger scale connectivity determines the nature of the stress transmission through particle suspension. To search for the microscopic origin of the stress fluctuations, we, therefore, consider the hierarchy of structures built up by particles that share frictional contacts with a minimum k neighbors. In the graph theory, this defines a contact graph (or network) composed of nodes with degree k at minimum [51,52]. As explained in the previous section, we define a neighbor, for each particle, as a particle close enough in proximity that it can interact with said particle by frictional forces. In our frictional model, this occurs when the sphere surfaces are in contact. The frictional force is proportional to the normal force between the neighboring spheres and acts to resist transverse motion relative to surface normal between neighboring spheres. We refer to particles with at least k neighbors as k-neighbor particles.

B. Constrained particle percolation

Testing k values from 2 to 6, we directly connect the percolation of k-neighbor particles to the rapid rise in viscosity and the large stress fluctuations corresponding to the DST. For each k, we identify the k-neighbor particles, sort them into clusters, obtain the cluster size distribution, and identify configurations in which at least one percolating cluster is

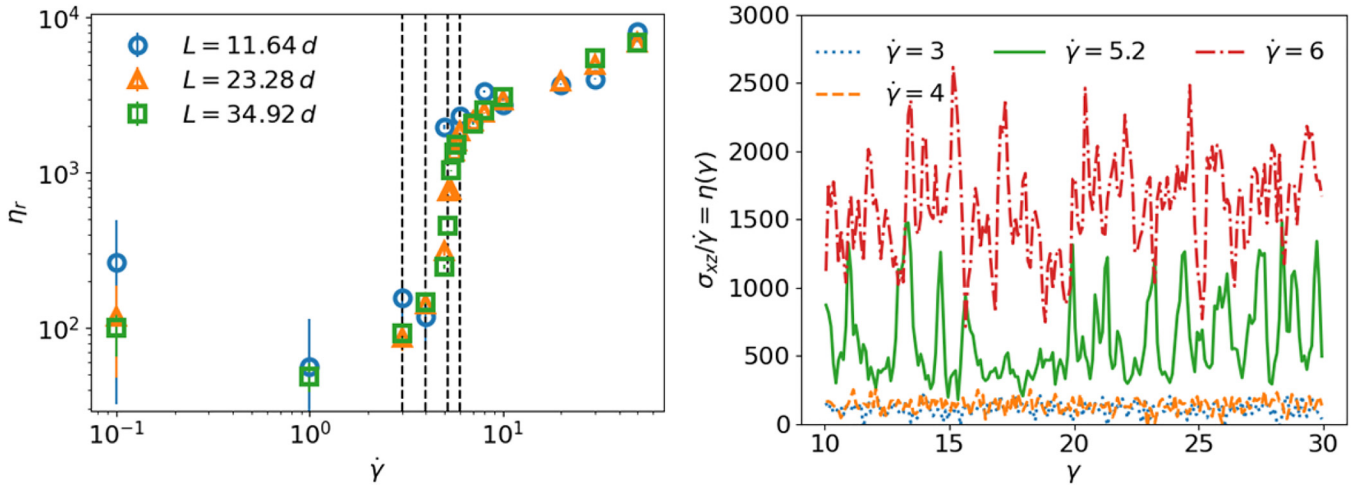

FIG. 2. (a) The average relative viscosity (η_r) as a function of shear rate ($\dot{\gamma}$) at $\phi = 56\%$ and different system sizes. The error bars represent one standard deviation from the mean calculated, after reaching steady state, from a running average over 25 strain units. The jump in the viscosity does not vary with increasing system size nor Reynolds number (albeit reducing Reynolds number produces a plateau at very high rates). The vertical dashed lines indicate the shear rates used in (b), showing instantaneous viscosity (stress/shear rate) as a function of applied strain γ. The jump in η_r is accompanied by large fluctuations of the stress near the critical shear rate.

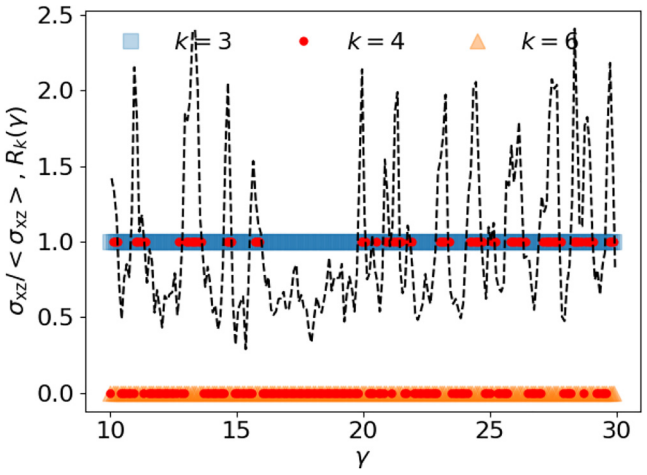

FIG. 3. $R_k(\gamma)$ (equal to 1 if a percolating cluster of k-neighbor particles exists and 0 otherwise) plotted for different k values alongside the stress $\sigma_{xz}/\langle\sigma_{xz}\rangle$ (dashed black line). The percolation of 4-neighbor particles corresponds to the giant stress fluctuations.

present in all directions. We have performed this analysis for all shear rates approaching the shear thickening transition in Fig. 2, and found that the percolation of 4-neighbor clusters is directly correlated to the stress fluctuations and DST. The plot in Fig. 3 superimposes the time series for the presence of a percolating cluster of k-neighbor particles ($R_k = 1$) or not ($R_k = 0$), for different k, to the time series of the shear stress close to DST ($\dot{\gamma} = 5.1$). The data show that clusters of 3-neighbor particles always percolate, independently from the stress fluctuations, which also happens for $k = 2$ (data not shown). In contrast, the percolation of a 4-neighbor cluster exactly corresponds to the spikes in the shear stress of the suspension. This behavior is confirmed across all shear rates around DST, whereas at low enough $\dot{\gamma}$, where DST does not occur and stress fluctuations are Gaussian, the percolation of 4-neighbor particles was not observed. Note, the 4-neighbor particles locally satisfy the Maxwell criterion for rigidity in the presence of tangential frictional forces [37]. At higher k values, percolation is significantly reduced for all shear rates. Indeed, Fig. 3 show that percolation of 6-neighbor particles, which, incidentally, correspond to locally rigid structures for frictionless spheres, does not occur close to DST. Our findings now strongly suggest that the self-organization of locally rigid, overconstrained particles into a percolating structure, reminiscent of shear jamming in granular fluids [53,54], is at the origin of the large stress fluctuations typical of DST, playing a significant role in this phenomenon. Indeed, the percolation of the rigid 4-neighbor particles can support the transmission of stress and bear most of the load also over an extended period of time, in contrast to k-neighbor particles with lower k values, which can be more easily disrupted. The percolation of the rigid 4-neighbor particles could, therefore, be central to the self-organization of the suspension microstructure under flow, when DST occurs.

C. Finite size scaling

Encouraged by these results, we now study the growth of 4-neighbor particle clusters using percolation theory. If a percolation transition emerges at a well-defined critical shear rate, we would like to identify the critical exponents which control the self-similar nature of the stress carrying structures, characterized by a linear size (or connectivity correlation length) that diverges approaching the transition. Recognizing that to extract such quantities is challenging even for static systems, here we expect additional challenges because of the highly dynamical nature of shear thickening systems.

We first try to determine if there is a critical shear rate that we could associate with a percolation threshold, by examining the probability of percolation, R, defined as the average occurrence of percolating clusters of 4-neighbor particles over each time series at different shear rates and for the three different system sizes. The data for R as a function of the shear rate (Fig. 4 inset) show, for all system sizes, a transition from 0 to 1. The larger the system size, the steeper the transition from 0 to 1 in probability, akin to the behavior of the percolation probability close to a percolation transition, where, due to finite size effects, the percolation probability increases earlier and the fluctuations smear out the transition region in smaller systems. With increasing system size, however, the transition region shrinks but does not significantly shift, suggesting that the percolation threshold of the 4-neighbor particles could indeed correspond to a specific, finite shear rate even in the limit of an infinite system. In percolation problems, a rough estimate of the percolation threshold (corresponding to the limit of an infinite system) can be obtained considering the point where the percolation probability curves for different system sizes intersect, which in our case corresponds to $\dot{\gamma}_c \approx 5$. $\dot{\gamma}_c$ points to a characteristic time scale over which a stable percolating network may be built or destroyed at a given shear rate. We expect this characteristic timescale to vary with the specific experimental system or microscopic parameters of the simulations (see appendix), as indeed observed for the DST threshold [20,23,47,55].

Close to a percolation transition, the percolation probability, and all other quantities related to the growth of

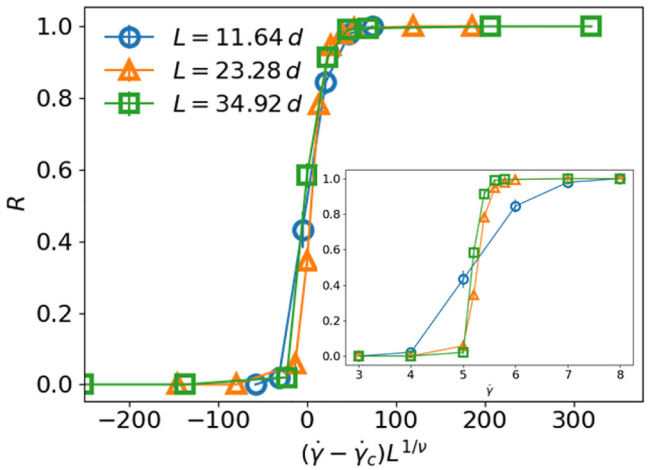

FIG. 4. Main frame: The probability R of 4-neighbor particles to form a percolating cluster as a function of the scaling variable $(\dot{\gamma} - \dot{\gamma}_c)L^{1/\nu}$ for three system sizes. Data collapse onto a unique curve for $\dot{\gamma}_c = 5.2$ and $\nu \approx 0.6$. Inset: The probability R of 4-neighbor particles to form a percolating cluster as a function of the shear rate for different system sizes.

connectivity, should follow the percolation finite size scaling *ansatz* [38]. That is, they vary with the distance from the transition threshold (in our case $\dot{\gamma}_c$) and the system size L only through a specific combination of both, which provides a scaling variable $(\dot{\gamma} - \dot{\gamma}_c)L^{1/\nu}$. In analogy with critical phenomena, the difference in the rate from the $\dot{\gamma}_c$ is related to a correlation length ξ in the system, which diverges at the percolation threshold with a critical exponent ν, and $(\dot{\gamma} - \dot{\gamma}_c)L^{1/\nu}$ can be interpreted as $(L/\xi)^{1/\nu}$. As in equilibrium critical phenomena, this property is the result of the self-similarity of a system close to a critical point [56], however, for percolation the property applies to a purely geometrical critical point related to the growth of connectivity. The finite size scaling *ansatz* provides the way to directly test the hypothesis that the system is indeed close to a percolation transition by verifying the presence of this regime for different quantities. Moreover, since the scaling variable and the scaling behavior depend on the critical exponents, one simultaneously obtains independent estimates of the critical exponents that describe their critical behavior.

Following percolation theory, we first attempt to collapse all the data for the percolation probability in terms of a scaling variable $(\dot{\gamma} - \dot{\gamma}_c)L^{1/\nu}$, which accounts for the statistical nature of percolation due to the system finite size, and where ν is the critical exponent that describes the divergence of the connectivity correlation length close to the percolation threshold. The data collapse obtained (Fig. 4, main frame) supports the validity of the finite size scaling *ansatz*. It only holds for a narrow range of values of the critical exponent ν, providing an estimate $\nu \approx 0.6$, and allows us to obtain a more accurate estimate of $\dot{\gamma}_c \approx 5.2$.

D. Estimating critical exponents

From the same cluster analysis of 4-neighbor particles, and having calculated the whole cluster size distribution, we can then compute the probability P of a 4-neighbor random particle being in the percolating cluster, the mean cluster size (i.e., the second moment of the cluster size distribution), and the maximum cluster size [38]. For all these quantities, the same finite scaling *ansatz* predicts that, once rescaled by a factor $L^{\alpha/\nu}$ where α is the specific critical exponent (with sign) for a given quantity, they only depend on $(\dot{\gamma} - \dot{\gamma}_c)L^{1/\nu}$. For example, since the probability P of a random particle being in the percolating cluster goes to 0 close to the percolation threshold $\dot{\gamma}_c$ as $(\gamma - \dot{\gamma}_c)^{\beta}$ in an infinite system, for any given finite system size L the same probability will follow the scaling $PL^{\beta/\nu} \propto (\dot{\gamma} - \dot{\gamma}_c)L^{1/\nu}$. For the mean cluster size S, which is the second moment of the cluster size distribution and diverges as $S \propto (\gamma - \dot{\gamma}_c)^{-\gamma}$ in an infinite system, the predicted scaling is $SL^{-\gamma/\nu} \propto (\dot{\gamma} - \dot{\gamma}_c)L^{1/\nu}$, and so on.

We can, therefore, test the finite size scaling *ansatz* by examining whether all data obtained in the simulations for different $\dot{\gamma}$ and different L indeed collapse onto a unique scaling function when plotted as a function of the scaling variable as it happened for the percolation probability just discussed. The occurrence of the data collapse is highly nontrivial and can be used to clearly identify the vicinity of a critical percolation regime.

Varying independently the values of critical exponents and percolation threshold across all three quantities, we identify the unique combinations producing the predicted data collapse [38] (Fig. 5). We note that we have significantly expanded the system sizes with respect to the existing literature on computational study of DST, however, we are far from being able to vary L by several orders of magnitudes, which would be required in this type of studies of critical behavior (Fig. 5, insets). Nevertheless, the evidence of the data collapse associated with a critical-like regime is striking (Fig. 5, main frames).

With this procedure, we confirm the estimated value $\nu \approx 0.6$ for the critical behavior of the correlation length, and independently determine the critical exponents $\beta \approx 0.18$, $\gamma \approx 1.3$, and $\sigma \approx 0.75$, respectively, describing the probability of a random particle to belong to a percolating cluster, the mean cluster size (related to the variance of the cluster size distribution), and the maximum cluster size. The exact determination of the critical exponents will require additional studies, but we note that the results obtained here show a significant discrepancy from the mean field values [56], and from those for the connectivity random percolation transition in $3D$ [38], suggesting that the percolation of the 4-neighbor particles during DST may correspond to a distinct universality class. Rigidity percolation studies, in which the percolation transition is associated to the growth of a rigid structure, are quite limited especially in $3D$ but do suggest a distinct

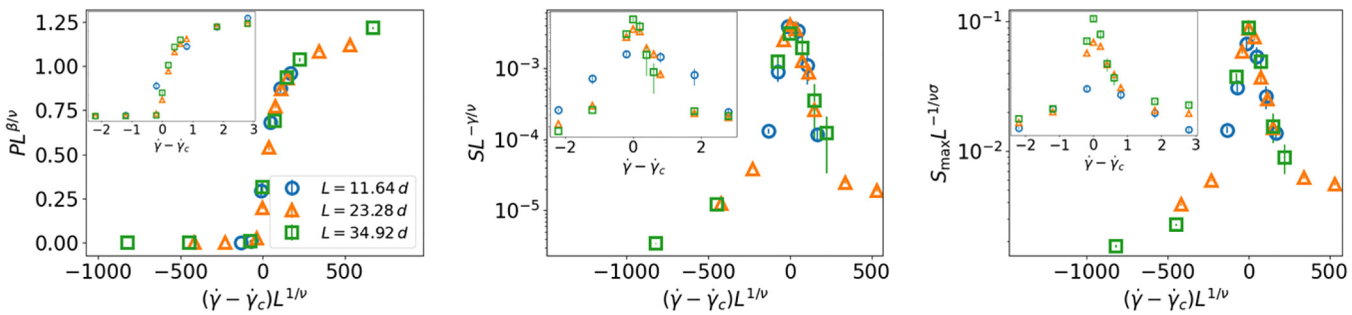

FIG. 5. Left: $PL^{\beta/\nu}$, with P the probability of a random 4-neighbor particle to belong to the percolating cluster, as a function of the scaling variable $(\dot{\gamma} - \dot{\gamma}_c)L^{1/\nu}$ and for different system sizes. Center: $SL^{-\gamma/\nu}$, with S the second moment of the cluster size distribution (or mean cluster size), as a function of $(\dot{\gamma} - \dot{\gamma}_c)L^{1/\nu}$. Right: $S_{\max}L^{-1/\nu\sigma}$, with $S_{\max}$ the maximum cluster size, as a function of $(\dot{\gamma} - \dot{\gamma}_c)L^{1/\nu}$ and for different system sizes. Using $\dot{\gamma}_c = 5.1$ obtained from the percolation probability (see Fig.3), data collapse for $\beta \approx 0.18$, $\sigma \approx 0.75$, and $\gamma \approx 1.3$. Insets: P (left), S (center), and $S_{\max}$ (right) plotted against $\dot{\gamma}$ for different system sizes.

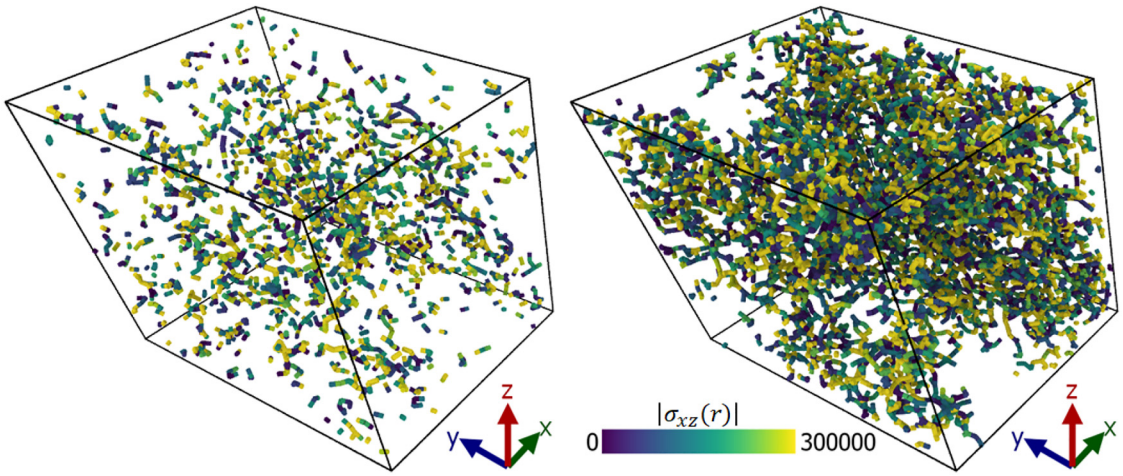

FIG. 6. Snapshots showing the frictional contacts between 4-neighbor particles at $\dot{\gamma} = 5$. The connections are colored by the magnitude of the local shear stress, $|\sigma_{xz}|$. In the left snapshot, $\sigma_{xz} \approx 500\, k_B T/d^3$, and we show all 4-neighbor particles. These are distributed homogeneously but do not percolate. The snapshot on the right corresponds to one of the spikes in the stress time series in Fig. 3. Here, only the percolating cluster is shown. The differences between these snapshots highlight the large microstructural rearrangements that can and do happen even in an apparent steady state.

universality class, and frictional rigidity percolation studies (in which frictional contacts are specifically included) found similar discrepancies [37,57].

Finally, we have also verified that varying the model parameters within a reasonable range shifts the DST threshold but does not seem to change the overall critical behavior (see appendix) [17,20,58]. We anticipate that modifying frictional constraints to include, for example, rolling friction [42], or varying the particle size distribution, may change the particle configurations that constitute locally rigid units, but we expect the percolation transition of said units to be robust.

IV. CONCLUSIONS

Using 3D simulations of particle suspensions, we have identified the microstructural units whose percolation corresponds to the onset of DST—providing the first direct evidence of a critical percolation transition underlying DST. These units build a locally rigid network of frictional contacts, and their cluster statistics follow the finite size scaling *ansatz* typical of critical phenomena and percolation theory. The percolation growth implies that, close to the percolation threshold, a few giant (percolating) clusters may coexist with a large number of large but non-percolating ones [38]. This coexistence could justify the viscosity, or the average shear stress, having a weak dependence on the system size [Fig. 2(a)], being dominated by the large number of non-percolating clusters. The fluctuations of the shear stress are, instead, distinctly controlled by the appearance of percolating clusters [see Figs. 2(b) and 3]. As also shown in Fig. 6, these fluctuations correspond to large microstructural rearrangements of 4-neighbor particles. Hence, the non-Gaussian nature of the large stress fluctuations is the consequence of spatially correlated rigid domains associated to percolating clusters of 4-neighbors particles.

Our findings call on experimental approaches to recognize the locally rigid structures, which, however, may be challenging even with stress field imaging [9,59,60]. Capability to identify the mechanical constraints acting locally on particles in the suspension contact network may be central to build on the insight gained here. As extensive simulations could allow, in the future, to precisely determine the universality class from the percolation exponents, experimental rheological tests and scaling analysis of experimental flow curves [19,23,30] could complement the microscopic understanding developed here. Following the hierarchical self-organization of k-neighbor particle structures under shear and identifying possible precursors of the rigidity percolation could provide novel insight into shear thickening instabilities.

There are several paths to expand on the work discussed here. For the high friction coefficient considered, any shear induced ordering [34] is completely disrupted, hence, we carried out our study for a monodisperse particle suspension, without recurring to a bidisperse or polydisperse mixtures [11,17,42,61]. With lower friction coefficients, however, or depending on the details of the particle contacts and boundaries, there could be some cases where some of degree of ordering survives in the presence of frictional contacts, as for example, also suggested by some experiments [62]. Another set of interesting questions concern the persistence of k-neighbor clusters and of their percolation behavior in the case of the continuous shear thickening regime (CST), where lubricated contacts play a more important role. Investigating the percolation of the k-neighbor clusters at different volume fractions, for example, will help us build a broader understanding of the flow induced organization of the particle microstructure in shear thickening suspensions.

ACKNOWLEDGMENTS

The authors thank the NIST PREP Gaithersburg Program (No. 70NANB18H151), NIST NRC Research Associateship Program, and National Science Foundation (No. NSF DMR-2026842) for support.

AUTHOR DECLARATIONS

Conflict of Interest

The authors have no conflicts to disclose.

DATA AVAILABILITY

The data that support the findings of this study are available from the corresponding author upon reasonable request.

APPENDIX: TIME SCALES

We tested the dependence of the DST on k_0 and η_0 to help gain insight into factors that may ultimately lead to the formation of the percolating structures herein described. Predictably, changing these parameters affected the critical rate at which DST was observed but does not seem to change the statistics of the 4-neighbor cluster close to the transition. We initially hypothesized that the shift in the critical rate might be explained by the changes in dimensionless numbers such as the Peclet number or Reynolds number (Re) but that does not seem to be the case in the flow regimes we studied.

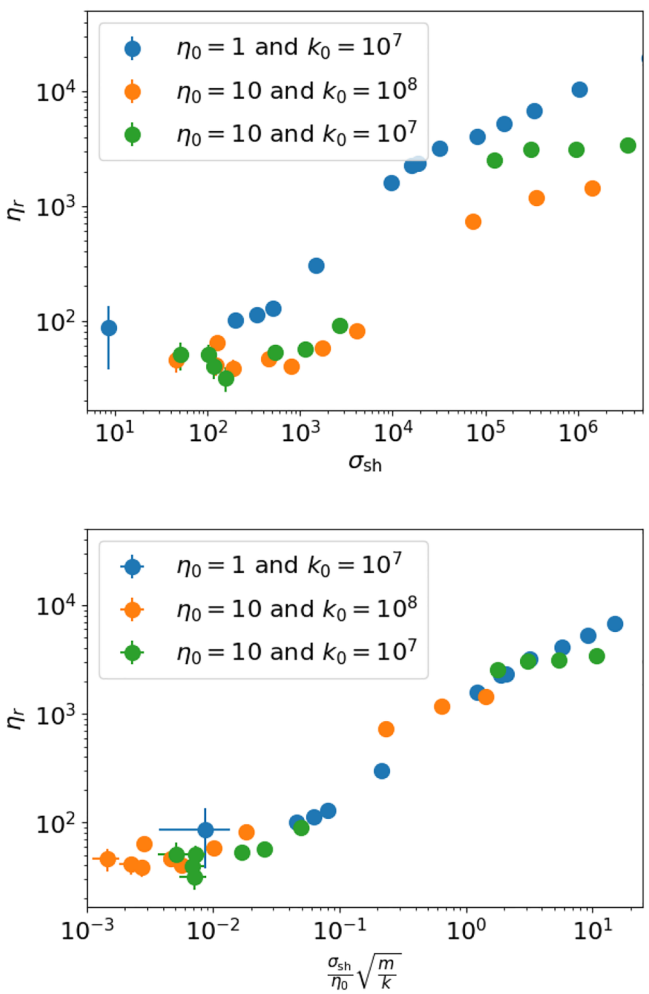

FIG. 7. Top: The relative viscosity plotted as a function of stress. The critical stress depends on parameters η_0 and k_0. Bottom: Rescaling the stress by η_0 and multiplying by the harmonic time scale $\sqrt{m/k}$ gives a dimensionless quantity which collapses the data to a single curve with a critical point close to 1.

However, it should be pointed out that increasing Re produces a gradual increase in viscosity for Re >1 . If we instead plot the relative viscosity vs the stress (Fig. 7), we can see that there appears to be a shift in the critical stress that is coupled to the value of η_0. From this, we began to consider other time scales in the system.

One inverse time scale could be constructed from the ratio σ/η_0. This is the shear rate we expect from the Newtonian solvent without any particles. The natural rate related to k_0 is the resonant frequency of our Hookean model, $\sqrt{k/m}$. Plotting η_r vs a dimensionless number given by the competition of these two rates $(\frac{\sigma}{\eta_0}\sqrt{\frac{m}{k}})$ produces a rather convincing data collapse, shown in Fig. 7. In addition, the DST transition appears close to $\frac{\sigma}{\eta_0}\sqrt{\frac{m}{k}} = 1$, suggesting that shear-rates sufficiently high compared to the particle spring frequency are needed to allow the build-up of a percolating and stress-bearing frictional network. Putting it another way, when the time scale of particle flow is sufficiently low compared to the time scale of particle contact, DST can occur.

REFERENCES

[1] Guazzelli, E., and J. F. Morris, *A Physical Introduction to Suspension Dynamics* (Cambridge University, New York, NY, 2012).
[2] Mewis, J., and N. J. Wagner, *Colloidal Suspension Rheology* (Cambridge University, New York, NY, 2011).
[3] Hoffman, R. L., "Discontinuous and dilatant viscosity behavior in concentrated suspensions. I. Observation of a flow instability," Trans. Soc. Rheol. **16**, 155–173 (1972).
[4] Leighton, D., and A. Acrivos, "The shear-induced migration of particles in concentrated suspensions," J. Fluid Mech. **181**, 415–439 (1987).
[5] Royer, J. R., D. L. Blair, and S. D. Hudson, "Rheological signature of frictional interactions in shear thickening suspensions," Phys. Rev. Lett. **116**, 1–5 (2016).
[6] Lootens, D., H. Van Damme, and P. Hébraud, "Giant stress fluctuations at the jamming transition," Phys. Rev. Lett. **90**, 178301 (2003).
[7] Hermes, M., B. M. Guy, W. C. K. Poon, G. Poy, M. E. Cates, and M. Wyart, "Unsteady flow and particle migration in dense, non-Brownian suspensions," J. Rheol. **60**, 905–916 (2016).
[8] Saint-Michel, B., T. Gibaud, and S. Manneville, "Uncovering instabilities in the spatiotemporal dynamics of a shear-thickening cornstarch suspension," Phys. Rev. X **8**, 031006 (2018).
[9] Rathee, V., D. L. Blair, and J. S. Urbach, "Localized stress fluctuations drive shear thickening in dense suspensions," Proc. Natl. Acad. Sci. U.S.A. **114**, 8740–8745 (2017).
[10] Xu, Q., A. Singh, and H. M. Jaeger, "Stress fluctuations and shear thickening in dense granular suspensions," J. Rheol. **64**, 321–328 (2020).
[11] Seto, R., R. Mari, J. F. Morris, and M. M. Denn, "Discontinuous shear thickening of frictional hard-sphere suspensions," Phys. Rev. Lett. **111**, 1–5 (2013).
[12] Mari, R., R. Seto, J. F. Morris, and M. M. Denn, "Shear thickening, frictionless and frictional rheologies in non-Brownian suspensions," J. Rheol. **58**, 1693–1724 (2014).
[13] Wyart, M., and M. E. Cates, "Discontinuous shear thickening without inertia in dense non-Brownian suspensions," Phys. Rev. Lett. **112**, 1–5 (2014).
[14] Lin, N. Y. C., B. M. Guy, M. Hermes, C. Ness, J. Sun, W. C. K. Poon, and I. Cohen, "Hydrodynamic and contact contributions to continuous

shear thickening in colloidal suspensions," Phys. Rev. Lett. **115**, 228304 (2015).
[15] Lootens, D., P. Hébraud, E. Lécolier, and H. Van Damme, "Gelation, shear-thinning and shear-thickening in cement slurries," Oil Gas Sci. Technol. **59**, 31–40 (2004).
[16] Morris, J. F., "Lubricated-to-frictional shear thickening scenario in dense suspensions," Phys. Rev. Fluids **3**, 110508 (2018).
[17] Jamali, S., and J. F. Brady, "Alternative frictional model for discontinuous shear thickening of dense suspensions: Hydrodynamics," Phys. Rev. Lett. **123**, 138002 (2019).
[18] Wang, M., S. Jamali, and J. F. Brady, "A hydrodynamic model for discontinuous shear-thickening in dense suspensions," J. Rheol. **64**, 379–394 (2020).
[19] Ong, E. Y. X., M. Ramaswamy, R. Niu, N. Y. C. Lin, A. Shetty, R. N. Zia, G. H. McKinley, and I. Cohen, "Stress decomposition in LAOS of dense colloidal suspensions," J. Rheol. **64**, 343–351 (2020).
[20] More, R. V., and A. M. Ardekani, "Effect of roughness on the rheology of concentrated non-Brownian suspensions: A numerical study," J. Rheol. **64**, 67–80 (2020).
[21] Nabizadeh, M., A. Singh, and S. Jamali, "Structure and dynamics of force clusters and networks in shear thickening suspensions," Phys. Rev. Lett. **129**, 068001 (2022).
[22] Sedes, O., A. Singh, and J. F. Morris, "Fluctuations at the onset of discontinuous shear thickening in a suspension," J. Rheol. **64**, 309–319 (2020).
[23] Ramaswamy, M., I. Griniasty, D. B. Liarte, A. Shetty, E. Katifori, E. Del Gado, J. P. Sethna, B. Chakraborty, and I. Cohen, "Universal scaling of shear thickening transitions," J. Rheol. **67**, 1189–1197 (2023).
[24] Seto, R., A. Singh, B. Chakraborty, M. M. Denn, and J. F. Morris, "Shear jamming and fragility in dense suspensions," Granular Matter **21**, 1–8 (2019).
[25] Sedes, O., H. A. Makse, B. Chakraborty, and J. F. Morris, "*k*-core analysis of shear-thickening suspensions," Phys. Rev. Fluids **7**, 024304 (2022).
[26] M. van der Naald, A. Singh, T. T. Eid, *et al.*, "Minimally rigid clusters in dense suspension flow," Nat. Phys. (published online, 2024).
[27] Thomas, J. E., K. Ramola, A. Singh, R. Mari, J. F. Morris, and B. Chakraborty, "Microscopic origin of frictional rheology in dense suspensions: Correlations in force space," Phys. Rev. Lett. **121**, 128002 (2018).
[28] Edens, L. E., E. G. Alvarado, A. Singh, J. F. Morris, G. K. Schenter, J. Chun, and A. E. Clark, "Shear stress dependence of force networks in 3D dense suspensions," Soft Matter **17**, 7476–7486 (2021).
[29] Gameiro, M., A. Singh, L. Kondic, K. Mischaikow, and J. F. Morris, "Interaction network analysis in shear thickening suspensions," Phys. Rev. Fluids **5**, 034307 (2020).
[30] Lin, N. Y. C., C. Ness, M. E. Cates, J. Sun, and I. Cohen, "Tunable shear thickening in suspensions," Proc. Natl. Acad. Sci. U.S.A. **113**, 10774 (2016).
[31] Xue, W., and G. S. Grest, "Shear-induced alignment of colloidal particles in the presence of a shear flow," Phys. Rev. Lett. **64**, 419 (1990).
[32] Bender, J., and N. J. Wagner, "Reversible shear thickening in monodisperse and bidisperse colloidal dispersions," J. Rheol. **40**, 899–916 (1996).
[33] Kulkarni, S. D., and J. F. Morris, "Ordering transition and structural evolution under shear in Brownian suspensions," J. Rheol. **53**, 417–439 (2009).
[34] Goyal, A., E. Del Gado, S. Z. Jones, and N. S. Martys, "Ordered domains in sheared dense suspensions: The link to viscosity and the disruptive effect of friction," J. Rheol. **66**, 1055–1065 (2022).
[35] Thorpe, M., D. Jacobs, M. Chubynsky, and J. Phillips, "Self-organization in network glasses," J. Non-Cryst. Solids **266**, 859–866 (2000).
[36] Liarte, D. B., X. Mao, O. Stenull, and T. C. Lubensky, "Jamming as a multicritical point," Phys. Rev. Lett. **122**, 128006 (2019).
[37] Liu, K., S. Henkes, and J. M. Schwarz, "Frictional rigidity percolation: A new universality class and its superuniversal connections through minimal rigidity proliferation," Phys. Rev. X **9**, 021006 (2019).
[38] Stauffer, D., and A. Aharony, *Introduction to Percolation Theory* (CRC, New York, NY, 2018).
[39] Mari, R., R. Seto, J. F. Morris, and M. M. Denn, "Discontinuous shear thickening in Brownian suspensions by dynamic simulation," Proc. Natl. Acad. Sci. U.S.A. **112**, 15326–15330 (2015).
[40] Singh, A., R. Mari, M. M. Denn, and J. F. Morris, "A constitutive model for simple shear of dense frictional suspensions," J. Rheol. **62**, 457–468 (2018).
[41] Plimpton, S., "Fast parallel algorithms for short – range molecular dynamics," J. Comput. Phys. **117**, 1–19 (1995).
[42] Singh, A., C. Ness, R. Seto, J. J. De Pablo, and H. M. Jaeger, "Shear thickening and jamming of dense suspensions: The "roll" of friction," Phys. Rev. Lett. **124**, 248005 (2020).
[43] Feys, D., G. De Schutter, S. Fataei, N. S. Martys, and V. Mechtcherine, "Pumping of concrete: Understanding a common placement method with lots of challenges," Cem. Concr. Res. **154**, 106720 (2022).
[44] Ball, R. C., and J. R. Melrose, "A simulation technique for many spheres in quasi-static motion under frame-invariant pair drag and Brownian forces," Phys. A **247**, 444–472 (1997).
[45] Morris, J. F., "Lubricated-to-frictional shear thickening scenario in dense suspensions," Phys. Rev. Fluids **3**, 1–16 (2018).
[46] Lee, Y.-F., Y. Luo, S. C. Brown, and N. J. Wagner, "Experimental test of a frictional contact model for shear thickening in concentrated colloidal suspensions," J. Rheol. **64**, 267–282 (2020).
[47] Singh, A., C. Ness, R. Seto, J. J. de Pablo, and H. M. Jaeger, "Shear thickening and jamming of dense suspensions: The "roll" of friction," Phys. Rev. Lett. **124**, 248005 (2020).
[48] Thompson, A. P., S. J. Plimpton, and W. Mattson, "General formulation of pressure and stress tensor for arbitrary many-body interaction potentials under periodic boundary conditions," J. Chem. Phys. **131**, 1–6 (2009).
[49] Hoshen, J., and R. Kopelman, "Percolation and cluster distribution. I. cluster multiple labeling technique and critical concentration algorithm," Phys. Rev. B **14**, 3438–3445 (1976).
[50] Evans, R., "Fluids adsorbed in narrow pores: Phase equilibria and structure," J. Phys.: Condens. Matter. **2**, 8989–9007 (1990).
[51] Morone, F., K. Burleson-Lesser, H. Vinutha, S. Sastry, and H. A. Makse, "The jamming transition is a k-core percolation transition," Phys. A **516**, 172–177 (2019).
[52] Papadopoulos, A., M. A. Porter, K. E. Daniels, and D. S. Bassett, "Network analysis of particles and grains," J. Complex Netw. **6**, 485 (2018).
[53] Dapeng, B., J. Zhang, B. Chakraborty, and R. P. Behringer, "Jamming by shear," Nature **480**, 355 (2011).
[54] Vinutha, H. A., and S. Sastry, "Disentangling the role of structure and friction in shear jamming," Nat. Phys. **12**, 578–583 (2016).
[55] Morris, J. F., "Shear thickening of concentrated suspensions: Recent developments and relation to other phenomena," Annu. Rev. Fluid Mech. **52**, 121–144 (2020).
[56] Goldenfeld, N., *Lectures on Phase Transitions and the Renormalization Group* (CRC, Nw York, NY, 1992).

[57] Jacobs, D. J., and M. F. Thorpe, "Generic rigidity percolation in two dimensions," Phys. Rev. E **53**, 3682–3693 (1996).

[58] Singh, A., S. Pednekar, J. Chun, M. M. Denn, and J. F. Morris, "From yielding to shear jamming in a cohesive frictional suspension," Phys. Rev. Lett. **122**, 098004 (2019).

[59] Jorjadze, I., L.-L. Pontani, and J. Brujic, "Microscopic approach to the nonlinear elasticity of compressed emulsions," Phys. Rev. Lett. **110**, 048302 (2013).

[60] Lin, N. Y. C., and I. Cohen, "Relating microstructure and particle-level stress in colloidal crystals under increased confinement," Soft Matter **12**, 9058–9067 (2016).

[61] More, R. V., and A. M. Ardekani, "Unifying disparate rate-dependent rheological regimes in non-Brownian suspensions," Phys. Rev. E **103**, 1–12 (2021).

[62] Miller, J. M., D. L. Blair, and J. S. Urbach, "Order and density fluctuations near the boundary in sheared dense suspensions," Front. Phys. **10**, 991540 (2022).